



HHS Public Access

Author manuscript

J Mater Chem B Mater Biol Med. Author manuscript; available in PMC 2017 May 28.

Published in final edited form as:

J Mater Chem B Mater Biol Med. 2016 May 28; 4(20): 3555–3561. doi:10.1039/C6TB00509H.

Bioactive Natural Protein–Hydroxyapatite Nanocarriers for Optimizing Osteogenic Differentiation of Mesenchymal Stem Cells

Z. Z. Ding^{a,b,#}, Z. H. Fan^{c,#}, X. W. Huang^{a,#}, S. M. Bai^a, D. W. Song^d, Q. Lu^{a,*}, and D. L. Kaplan^{a,e}

^aNational Engineering Laboratory for Modern Silk and Collaborative Innovation Center of Suzhou Nano Science and Technology, Soochow University, Suzhou 215123, People's Republic of China

^bSchool of Biology and Basic Medical Sciences, Soochow University, Suzhou 215123, People's Republic of China

^cDepartment of Orthopedics, The Second Affiliated Hospital of Soochow University, Suzhou 215000, People's Republic of China

^dTai'an City Central Hospital, Taian 271000, People's Republic of China Address

^eDepartment of Biomedical Engineering, Tufts University, Medford, MA 02155, United States

Abstract

Improving the controlled release of bioactive growth factors to regulate cell behavior and tissue regeneration remains a need in tissue engineering and regenerative medicine. Inorganic and polymeric nanoparticles have been extensively fabricated as bioactive biomaterials with enhanced biocompatibility and effective carriers of therapeutic agents, however, challenges remain such as the achievement of high loading capacity and sustained release, and the bioactivity preservation of growth factors. Here, a multilayered, silk coated hydroxyapatite (HA) nanocarrier with drug loading-release capacity superior to pure silk or HA nanoparticles was developed. Bone morphogenetic protein-2 (BMP-2) was bound to the silk coatings with a high binding efficiency of 99.6%, significantly higher than that in silk or the HA nanoparticles alone. The release of BMP-2 was sustained *in vitro* over a period of 21 days without burst release. Compared with BMP-2 loaded silk or HA particles, bone mesenchymal stem cells (BMSCs) showed improved proliferation and osteogenesis when cultured with the BMP-2 loaded composite nanocarriers. Therefore, these silk-HA composite nanoparticles present a useful approach to designing bioactive nanocarrier systems with enhanced functions for bone tissue regeneration needs.

Introduction

With an increase in demand for therapies that are able to repair large bone defects, tissue engineering is attracting more attention and the use of nanomaterials is of interest for targeted drug delivery and potential to provide additional cues to direct cell differentiation

*Qiang Lu, Tel: (+86)-512-67061649; Lvqiang78@suda.edu.cn.

#The authors have same contribution

and facilitate the regeneration of functional bone tissue.^{1–4} Different nanoscale materials that achieve controlled release of bioactive drugs have been reported for musculoskeletal tissue engineering, including polymeric nanoparticles consisting of micelles and dendrimers, and inorganic nanoparticles such as calcium phosphate and bioactive glasses.^{5–9} Calcium phosphates (CaP), particularly hydroxyapatite (HA), have similar chemical and crystallographic structures with the inorganic components of bone *in vivo* and are used in orthopedic applications^{10–12} Their excellent biocompatibility and osteo-conductivity make them important candidates for bone regeneration and the delivery of growth factors.^{13–15} Different processes were developed to tune the morphology, size and structure of HA nanoparticles to improve drug loading and release properties.^{16–18} However, additional steps to remove surfactants, significant reaction time and special processing equipments are usually required for these procedures.^{16–18} Low drug loading capacity and quick release behavior remain major challenges for HA-based delivery systems.

Silk, a natural protein, has been applied as a carrier for the controlled release of growth factors due to its outstanding biocompatibility and biodegradability.^{19–21} Silk carriers controlled the loading and release of different growth factors without the compromise of their bioactivity.^{22,23} Several methods have also been used to fabricate silk nanoparticles to achieve tunable release behavior.^{23,24} Unlike HA nanoparticles, silk carriers show high loading capacity and slower release rate for different growth factors.²³ However, the silk nanoparticles are usually metastable. It still remains a challenge to prepare stable water-dispersible silk nanoparticles to load the growth factors. Silk is also not osteoconductive and therefore can't stimulate osteogenesis of bone marrow derived mesenchymal stem cells (BMSCs).^{25,26} Thus, the design of silk-HA composite delivery systems was pursued, with the advantages of both components to improve osteogenic differentiation of BMSCs. Recently, water-dispersible HA nanoparticles were developed with silk as template and surface stabilizer.²⁷ The nanoparticles with core-shell structures are appropriate for drug delivery.²⁷ An all-aqueous mild fabrication process makes the nanoparticles suitable for loading sensitive growth factors. Therefore, a facile approach is developed to load bone morphogenetic protein 2 (BMP-2) in the silk-HA nanoparticles. The prepared BMP-2 loaded samples exhibit higher loading efficiency and sustained release than pure silk or pure HA nanocarriers. Improved osteogenic differentiation of BMSCs suggests the feasibility of designing composite nanocarriers with optimized functions for bone regeneration.

Experimental

Preparation of aqueous silk solutions

A previously published procedure *was used to prepare Bombyx mori* silk solutions.^{28–30} Silks were boiled in 0.02 M aqueous Na₂CO₃ solution for 20 min, and then rinsed thoroughly with distilled water to extract the residual sericin. The extracted silk was placed in 9.3 M LiBr solution at 60°C for 4 h to achieve a 20% (w/v) solution. This solution was loaded in Slide-a-Lyzer dialysis cassettes (Pierce, MWCO 3,500) and dialyzed against distilled water for 72 h to remove the salt. After dialysis, the solution was centrifuged at 9,000 rpm for 20 min at 4°C and finally achieved optically clear silk solution with concentration of about 6 wt%.

Fabrication of nanocarriers

Silk-HA nanoparticles were synthesized via a modified aqueous precipitation reaction in which silk was used as template and surface stabilizer.²⁷ The silk nanoparticles with homogeneous size were prepared through incubating fresh silk solution (6 wt %) at 60°C for 24 h. 20 mL H₃PO₄ solutions (0.06 M) were blended with 20 mL of silk nanoparticle solution to form the mixed solution. Then the mixed solution was added to 100 mL Ca(OH)₂ suspensions (0.02 M) with dropping speed of 90 mL h⁻¹ along with vigorous stirring. The solution was cultured in a water bath at 70°C, following pH adjustment with 0.1 M NaOH. Finally, the silk-HA nanoparticles were prepared after the centrifugation at 9,000 rpm for 20 min and the washing treatment with distilled water. As a control, the silk-HA nanoparticles were treated at 550°C in a muffle furnace for 2 h to get pure HA particles after further three washing processes with distilled water. Pure silk nanoparticles were also fabricated using a modified method.³¹ The fresh silk solution (100 µl, 15 µg/µl) was thoroughly mixed with ethanol (40 µl), then mixed with poly(vinyl alcohol) (PVA, 2 ml, 2% w/v) and vortex for 10 s. After freezing at -20 °C for 20 h and defrosting at room temperature, the mixture became a milky emulsion. Eventually, the dry silk particles were obtained by centrifugation (12,000 rpm, 5 min) and lyophilization.

BMP-2 loading and release

For loading, 1.5 mg of silk-HA nanoparticles, pure silk nanoparticles and pure HA particles were incubated in 1 mL 15 µg/mL BMP-2 solution (Ruibang Company, Shanghai, China) at 4 °C for 24 h. The products were collected by centrifugation at 12,000 rpm for 3 min and all the supernatants were preserved. A BMP-2 ELISA kit (Biovision, San Francisco, CA) was used to measure the BMP-2 content in the supernatant solution based on the manufacturer's instructions. The loading efficiency of BMP-2 was obtained according to the following formula:

$$\text{Loading efficiency} = (W_0 - W_1) / W_0 \times 100\%$$

Where W_0 is the total weight of BMP-2 in the reaction, W_1 is the total weight of free BMP-2 remaining in the supernatant. The data that are obtained from the triplicate measurements of the different samples are showed as mean ± standard deviation.

BMP-2 loaded particles (5 mg) were added into PBS solution (pH 7.4, 1mL) and cultured in a thermostatic shaker at 37 °C to study the release behaviors. At designed time, the supernatant (1 mL) was taken out for the following BMP-2 content analysis through a BMP-2 ELISA kit (Biovision, San Francisco, CA). Fresh PBS buffer solution (1 mL) was supplied into the release medium. The experiments were repeated in triplicate from different samples.

The BMP-2 was also labelled with fluorescein-5(6)-carboxamidocaproic acid N-succinimidyl ester (FITC) to further investigate loading efficiency. Here 30 µg of FITC was added into 3 mL BMP-2 aqueous solution (1.5 mg/mL, clinical grade, Medtronic, Minneapolis, MN). The mixture was cultured for 24 h at 4°C. Then, FITC-labelled BMP-2 (FITCBMP-2) was gathered with a concentrator (10K, Pierce, Grand Island, NY) and re-

dispersed to 3 mL. FITC-labelled BMP-2 was loaded into the particles using the above said protocols.

Characterization

A scanning electron microscope (SEM, S-4800, Hitach, Tokyo, Japan) was used to study the morphology of the nanocarriers at the voltage of 3.0 kV after gold sputter coating. The composition in the nanocarriers was analyzed by Fourier transform infrared spectroscopy (FTIR, Nicolet 5700, ThermoScientific, FL, America) in the spectral region of 400–4000 cm^{-1} . X-ray diffraction (XRD, X' Pert-Pro MPD, PANalytical BV, Almelo, Holland) was applied to analyze the crystal structure. X-rays were produced at 30 mA and 40 kV, and data were collected at diffraction angles from 10 to 60°. The step size and scanning speed were 0.02° and 6°/min, respectively. The size distribution and zeta potential of the nanocarriers were measured using Zetasizer Nanoseries (Nano ZS90, Malvern instruments, Malvern, UK). Each sample was repeated five times at 25 °C, and the mean \pm standard deviation (n=5) were calculated. Fluorescence images of the FITCBMP-2-loaded silk nanoparticles, HA particles and silk-HA nanoparticles were captured by a fluorescence inverted microscope (AxioVert A1, ZEISS, Oberkochen, Germany).

In vitro biocompatibility of the nanocarriers

BMSCs derived from Sprague-Dawley (SD) rats were cultured *in vitro* to assess the biocompatibility of the nanocarriers. All animal procedures followed the ethical guidelines of the experimental animals approved by Institutional Animal Care and Use Committee, Soochow University. Briefly, BMSCs and nanocarriers (BMP-2 free nanocarriers and nanocarriers loaded with 300 ng of BMP-2) were incubated in a 15 mL polypropylene round tube. After 2 h of incubation, the cells were moved to 6 well plates with 5×10^5 BMSCs in each well. As a control, cell pellets were also cultured in Dulbecco's modified Eagle medium that contained 300 ng/mL soluble BMP-2.

The proliferation behavior of the BMSCs was studied by DNA content assay on day 1, 3, and 7. Before the measurement, samples were treated with proteinase K overnight at 56°C to digest the remained scaffolds.²⁸ The DNA content was measured using the PicoGreen™ DNA assay according to the protocol of the manufacturer (Invitrogen, Carlsbad, CA). A standard curve over a range of concentrations was firstly prepared with λ -phage DNA in 10×10^{-3} M Tris-HCl (pH 7.4), 5×10^{-3} M NaCl, 0.1×10^{-3} M EDTA. Then the amount of DNA data was collected at an excitation wavelength of 480 nm and emission wavelength of 530 nm using a BioTeK Synergy 4 spectrofluorometer (BioTeK, Winooski, VT) and calculated based on the standard curve.

Cell morphology was observed by confocal laser scanning microscope (CLSM, Olympus FV10 inverted microscope, Nagano, Japan). Samples for CLSM observation were initially washed in phosphate buffer, fixed with 4% paraformaldehyde solution (Sigma-Aldrich, St. Louis, MO) for 30 min, and then were washed and permeabilized with 0.1% Triton X-100 for 5 min. Samples were stained with FITC-phalloidin (Sigma-Aldrich, St. Louis, MO) and DAPI (Sigma-Aldrich, St. Louis, MO), after which the fluorescence signals were visualized.

***In vitro* cell differentiation on the nanocarriers**

For osteogenic differentiation, BMSCs (5×10^5 cells per well) were seeded and cultured as above. Briefly, the groups of particles loaded 300ng of BMP-2 were centrifuged inside 15 ml tubes. 5×10^5 BMSCs were dispersed in the medium (1 mL) and then gently added to the tubes for the further centrifugation. After seeded on the different particle samples, the MSCs were cultured in an osteogenic medium supplemented with L-ascorbic acid (50mM) and β -glycerophosphate (10mM). The medium also contained Glucose Dulbecco's modified Eagle's medium, 10% FBS, and 1% penicillin/streptomycin. As a control, cell pellets were also cultured in soluble BMP-2-contained osteogenic medium (BMP-2, 300ng/ml). After 7 d, alkaline phosphatase (ALP) assay, quantification of calcium content, bone-related gene expression and immunofluorescence staining were performed. For alkaline phosphatase activity, cell lysates were firstly centrifuged. Then the supernatant was diluted into 80 μ L and mixed with 50 μ L of 5 mM p-nitrophenol phosphate substrate. After incubated in a 96-well plate at 25°C for 1 h, 20 μ L of NaOH solution (2 M) was added in the mixture to stop the reaction. The production of p-nitrophenol was calculated according to the absorbance intensity at 405 nm on a microplate reader and the ALP activity was normalized based on the total protein content that could be determined by Bradford protein assay. In order to avoid the possible influence of calcium in solution, the cultured cells were centrifuged from the solution and then the calcium content inside the cell lysates was measured using a calcium colorimetric assay kit (Biovision, San Francisco, CA) according to the manufacturer's instructions. For bone-related gene expression (Runx2 and osteocalcin), total cellular RNA was extracted with Trizol reagent (Invitrogen, Carlsbad, CA) and then purified using the RNeasy Mini Kit (Applied Biosystems, Carlsbad, CA). The RNA concentration was measured with Nano Drop 2000 (Thermo Scientific, Waltham, MA). A High Capacity cDNA Reverse Transcription kit (Applied Biosystems, Carlsbad, CA) was used and successfully reverse transcribed 1 mg of the extracted total RNA into complementary DNA (cDNA) with a 2720 thermal cycler (Applied Biosystems, Foster City, CA). Real-time PCR results were obtained through a 7500 Real-Time PCR System (Applied Biosystems, Foster City, CA) with the Fast SYBR Green kit (Applied Biosystems, Carlsbad, CA). The PCR reaction conditions were as follows: 95°C (20 s), 40 cycles at 95°C (3 s), and 60°C (30 s). The expression level of the target gene was normalized to glyceraldehyde-3-phosphate dehydrogenase (GAPDH), and then calculated based on the 2^{-Ct} formula with reference to the respective control group. Immunofluorescence staining of collagen I was also applied to assess the osteogenic differentiation capacity of the samples. After washed with phosphate buffer, the samples were fixed with 4% paraformaldehyde solution (Sigma-Aldrich, St. Louis, MO) for 30 min, permeated with 1% Triton X-100 for 30 min and blocked with 3% rabbit for 30 min at room temperature. Then, primary antibody (Anti-Collagen I antibody; Abcam, Cambridge, MA) were incubated with the samples overnight at 4°. After washing three times with PBS, samples were cultured with secondary antibody (Goat Anti-Rabbit immunoglobulin G; Invitrogen, Carlsbad, CA) for 60 min and finally incubate with DAPI (Sigma-Aldrich, St. Louis, MO) for 3 min. Representative fluorescence images (20 \times) of stained samples were achieved by CLSM (Olympus FV10 inverted microscope, Nagano, Japan) with excitation/emission at 358/461 (488/568) and 494/518 nm.

Statistical analysis

SPSS v.16.0 software was performed to make the statistical analyses. Two-way A OVA followed by the Student-Newman-Keuls test (SNK q test) was used to analyse the mean values of the data sets. Unless otherwise specified, the data are presented as means \pm standard deviations, and $p < 0.05$ is considered statistically significant.

Results and discussion

Silk-HA composite nanoparticles were synthesized with silk as the template and stabilizer. According to our previous study,²⁷ these composite nanoparticles had a core-shell structure where the silk coating could form strong interactions with BMP-2 to achieve higher loading capacity (Fig 1Aa). As a control, the composite nanoparticles were treated at 550 °C for 2 h to generate pure HA nanoparticles, eliminating the organic components but not altering the micro-morphology of the particles (Fig 1Ab). Pure silk nanoparticles with a similar size were also prepared (Fig 1Ac).³¹

The composite particles formed were nanorods with size of about 65 nm wide and 150–200 nm long, whereas the silk nanoparticles were spheres with diameter around 155 nm (Figure 1A, B). Although the morphology of HA particles maintained unchanged after the removal of the silk, aggregation into larger particles occurred due to the elimination of repulsive forces from silk.²⁷ The FTIR spectra and XRD pattern (Fig 1C, D) showed typical silk and HA characteristic peaks for the composite particles, suggesting the co-existence of HA and silk in the particles. Then the peaks attributed to silk disappeared after thermal treatment, confirming the removal of the silk. Therefore, silk-HA composite particles, pure HA particles and pure silk particles with similar sizes were prepared for BMP-2 loading and release studies.

To observe BMP-2 incorporation behavior on the different particles, fluorescein isothiocyanate (FITC)-labelled BMP-2 samples were prepared after the particles were separately soaked in FITCBMP-2 solution for 24 h, collected by centrifugation, and washed twice with water to remove non-absorbed BMP-2. Figure 2 A–C showed fluorescent microscopy images for FITCBMP-2 loaded particles. Emission of green fluorescence indicated successful loading of BMP-2 on the samples.³² The fluorescence intensity for silk and silk-HA nanoparticles were significantly higher than that for the pure HA particles, suggesting higher BMP-2 loading on silk and silk-HA nanoparticles. When the initial loading was 1% (BMP-2: nanocarriers = 1:100, w/w), the loading efficiency of BMP-2 was about $60.5 \pm 5.98\%$ for pure HA particles and increased to $96.5 \pm 1.64\%$ for the pure silk particles, which is similar to that reported previously.²³ Since the BMP-2 was loaded on the surface of the particles through the present a sorption method, the loading capacity was depended on silk rather than HA. Therefore, similar to the silk carriers, the silk-HA composite particles showed good BMP-2 loading efficiency, which was $99.6 \pm 0.35\%$. Several studies have revealed high loading capacity for silk-based nanoparticles due to the electrostatic charge interaction between silk and BMP-2.^{23,25} Compared to pure silk nanoparticles (-15.98 ± 0.18 mV), higher zeta potential (-17.13 ± 0.11 mV) was achieved for the composite nanoparticles, which might result in the further improvements in loading capacity. Silk nanofibers with higher negative charge (zeta potential -50 mV) were prepared

in our group and also showed excellent BMP-2 absorption, confirming our assumption (data not shown). The results indicated that the low loading capacity, a main challenge for HA-based carriers, was successfully resolved in our nanocarrier system by incorporating the silk coating.

BMP-2 delivery from the materials was studied to ascertain the release characteristics (Figure 2E–F), which is important for assessing delivery potential.^{33,34} Similar to other HA nanoparticles,¹⁷ the HA particles exhibited a typical burst release of BMP-2, with up to 90% released after only 2 h. Unlike the HA particles, both the silk and silk-HA composite particles showed slower and sustained release behaviors without an initial burst release. Even after 21 days, only about 50% and 70% of BMP-2 was released from silk and silk-HA composite nanoparticles, respectively. Although the silk-HA composite nanoparticles showed slightly faster release rate than the silk particles, more stable and linear release behaviors were found with the composite particles (Fig 2F). A burst release of BMP-2 has significant adverse biological effects, such as nerve damage, immunological responses, and even unfavorable bone formation.^{25,33–35} Recent studies revealed that silk carriers minimized the cytotoxicity of BMP-2 with the preservation of activity, a feature that is improved over pure HA nanoparticles.^{23,25} The silk-HA composite nanocarriers retained suitable loading/delivery properties of silk-based carriers, suggesting promising potential for osteogenic differentiation and bone tissue engineering by including the three components in the system (silk, HA, BMP-2).

Since HA is stable and hard to be degraded within short term the released calcium ions were never detected when the HA-silk composite nanoparticles were cultured in water for above two weeks at 37°C. The influence of calcium ions on cell behaviors could be negligible in our present study. DNA content was used to evaluate cell compatibility. Since 300 ng/ml BMP-2 leads to good proliferation of MSCs,^{23,25} free BMP-2 at concentration of 300 ng/ml was used as a control. The DNA content gradually increased for all samples (Figure 3) and there was no significant difference among the samples within three days, suggesting cell compatibility. Differences in cell proliferation occurred after 7 days where the BMP-2 loaded silk particles supported similar proliferation with the samples containing soluble BMP-2, but higher proliferation was achieved for the BMP-2 loaded HA particles and silk-HA composite particles. These results suggested that the presence of HA further improved the biocompatibility of the nanocarriers, which was also revealed in previous studies.^{10–12,27} Although further investigation was necessary, it was suggested that the organic-inorganic silk-HA composite structures, similar with natural bone microenvironment, provided better niche for the MSCs. Similar results was also found on silk-HA composite scaffolds, where the MSCs proliferated better on the composite scaffolds than on the pure silk scaffolds.²⁷ These results imply that the composite nanocarriers minimized cytotoxicity effects due to BMP-2, and also accelerated cellular proliferation compared to pure silk materials.

The particles were subsequently used in cellular differentiation studies. The silk particles, HA particles and silk-HA composite particles with and without BMP-2 were termed Silk-BMP, HA-BMP, Silk-HA-BMP, Silk, HA and Silk-HA, respectively. As control, the free BMP-2 as termed BMP-2. The osteogenic differentiation of BMSCs was firstly assessed with ALP activity, an early marker of osteogenesis.³⁶ Without BMP-2 factor, the cells

showed higher ALP expression on the particles containing HA than on the pure silk particles, suggesting the osteoinductive property of HA (Fig 4A). Then the ALP expression was improved after the addition of free BMP-2 and further enhanced when the cells were cultured on different BMP-2 loaded particles because of the controlled release of BMP-2. Highest expression was achieved on HA-BMP samples since the quick release of BMP-2 from the HA-BMP samples resulted in higher BMP-2 concentration than the Silk-BMP and Silk-HA-BMP samples. Then, calcium production by the differentiated MSCs correlated with the potential of osteogenesis,³⁷ was investigated (Fig 4B). Unlike the ALP expression, free BMP-2 had negligible influence on calcium content. The calcium content of the cells cultured with free BMP-2 was even lower than that cultured with HA and silk-HA samples without BMP-2. The results indicated that free BMP-2 hardly accelerate later osteodifferentiation might because of rapid diffusion and degradation of free BMP-2 that have been reported previously.²⁵ Compared to free BMP-2, the BMP-2 loaded on different particles could maintain its bioactivity and result in significantly higher calcium mineralization. Highest calcium content was observed on Silk-HA-BMP samples, suggesting that the composite BMP-2 carriers maintained both the advantages of HA (osteoinductive property) and silk (sustained release and bioactivity preservation of BMP-2). Although HA, as the core material, can't interact with the cells directly, the mechanical signals of the A particles should influence the cell behaviors, resulting in the better osteogenic differentiation.

Gene expression of RUNX2 and osteocalcin were quantified by qRT-PCR to further assess the osteogenic differentiation of BMSCs after the cells were cultured for a week.²³ RUNX2, marker for the transition from stem cell to osteocyte,^{25,38} was investigated to assess osteodifferentiation of BMSCs (Fig 4C). Compared to that on pure silk particles, the cells showed significantly higher RUNX2 expression on free BMP-2, HA particles and silk-HA particles, confirming the osteoinductive capacity of HA and BMP-2. RUNX2 expression on the three BMP-2 loaded particle groups was significantly higher than on the corresponding BMP-2 free particles (Figure 4C). The results indicated that the BMP-2 loaded on the different particles could maintain bioactivity and facilitated RUNX2 expression. Although the BMP-2 released quickly from pure HA particles, the cells cultured on HA-BMP samples expressed higher RUNX2 than that cultured on silk-BMP samples, which should be due to the synergistic effect of HA and BMP-2. Therefore, highest RUNX2 expression was achieved on the silk-HA-BMP samples since the samples had better BMP-2 release property without the sacrifice of HA osteo-inductivity. Osteocalcin, a noncollagenous protein secreted by osteoblasts,^{39,40} was upregulated in all the particles containing HA. Similar results were also observed with previous HA-based nanoparticles, supporting the bioactivity and osteoinductivity of HA nanoparticles.^{10-12,14} Compared pure silk particles, higher expression of osteocalcin occurred the silk-HA composite particles without the loading of BMP-2 which suggested that the upregulation of osteocalcin should be due to the HA existence. The controlled release of BMP-2 could also improve the upregulation of osteocalcin. Osteocalcin expression was further increased following BMP loading, achieving the highest expression in the BMP-2 loaded silk-HA composite particles (Figure 4D). Immunofluorescence staining was also performed to detect the expression of collagen I, a useful marker for osteogenic differentiation of the BMSCs in some previous studies.^{37,41}

Although it is not a very good specific marker for osteogenic differentiation, the highest expression of collagen I was observed in the BMP-2-loaded silk-HA composite nanoparticles (Figure 5). The results were coincident with the PCR results, confirming the best osteoinductivity with these particles. Hence, although further investigation is necessary to clarify the specific influence of HA and BMP-2 in our system, our present results confirmed that the silk-HA composite nanocarriers could possess both the strong points of HA and silk carriers, resulting in improved osteogenic differentiation. The higher efficacy of BMP-2 delivery and better osteoinductivity make these composite nanoparticles suitable for bone regeneration.

Conclusions

A protein-HA composite nanocarrier to enhance the delivery and function of BMP-2 is reported. The nanocarrier demonstrated suitable BMP-2 loading efficiency, significantly higher than the pure silk and pure HA nanoparticles. The composite particles also showed longer delivery of BMP-2 in comparison to the HA nanoparticles reported previously. The nanocarriers possessed significantly better osteoinductivity than pure silk and HA nanoparticles. The sustained release of BMP-2 loaded in the nanocarriers resulted in improved upregulation of markers associated with osteogenic differentiation of BMSCs in comparison to pure silk and HA nanocarriers. These composite nanoparticles may have utility in injectable matrices, bioactive fillers, and therapeutic agents for bone-related tissue regeneration. Further, the combination design for these nanocarriers provides an important strategy to optimize properties for targeted applications, exploiting the utility of each component as well as the synergy in binding and distribution by utilizing the combination.

Supplementary Material

Refer to Web version on PubMed Central for supplementary material.

Acknowledgments

The authors thank National Basic Research Program of China (973 Program, 2013CB934400), NSFC (21174097, 51403144) and the NIH (R01 DE017207, P41 EB002520). We also thank the Priority Academic Program Development of Jiangsu Higher Education Institutions (PAPD), the Excellent Youth Foundation of Jiangsu Province (BK2012009), the Natural Science Foundation of Jiangsu Province (Grants No BK20140397, BK20140401), and the Key Natural Science Foundation of the Jiangsu Higher Education Institutions of China (11KGA430002) for support of this work.

Notes and references

1. Zheng CP, Wang JS, Liu YN, Yu QQ, Liu Y, Deng N, Liu J. *Adv. Funct. Mater.* 2014; 24:6872.
2. Balmert SC, Little SR. *Adv. Mater.* 2012; 24:3757. [PubMed: 22528985]
3. Kumar A, Zhang X, Liang XJ. *Biotechnol. Adv.* 2013; 31:593. [PubMed: 23111203]
4. Guo JF, Cahill MR, McKenna SL, O'Driscoll CM. *Biotechnol. Adv.* 2014; 31:1396. [PubMed: 25218571]
5. Colson YH, Grinstaff MW. *Adv. Mater.* 2012; 24:3878. [PubMed: 22988558]
6. Li L, Zhou GL, Wang Y, Yang G, Ding S, Zhou SB. *Biomaterials.* 2015; 37:218. [PubMed: 25453952]
7. Zhao Y, Zhou YX, Wang DS, Gao YJ, Li JW, Ma SJ, Zhao L, Zhang C, Liu Y, Li XR. *Acta Biomater.* 2015; 17:182. [PubMed: 25612838]

8. Oliveria JM, Kotobuki N, Tadokoro M, Hirose M, Mano JF, Reis RL, Ohgushi H. *Bone*. 2010; 46:1424. [PubMed: 20152952]
9. Miguez-Pacheco V, Hench LL, Boccaccini AR. *Acta Biomater*. 2015; 13:1. [PubMed: 25462853]
10. Bongio M, van den Beucken JJ, Nejadnik MR, Thamasebi BZ, Habibovic P, Kinard LA, Kasper FK, Mikos AG, Leeuwenburgh SCG, Jansen JA. *Acta Biomater*. 2013; 9:5464. [PubMed: 23107797]
11. Grover LM, Wright AJ, Gbureck U, Bolarinwa A, Song JF, Liu Y, Farrar DF, Howling G, Rose J, Baralet JE. *Biomaterials*. 2013; 34:6631. [PubMed: 23747007]
12. Liu X, Wang P, Chen WC, Weir MD, Bao CY, Xu HH. *Acta Biomater*. 2014; 10:4484. [PubMed: 24972090]
13. Sachiko H, Motoki I, Tetsushi T, Misao Y, Naofumi O. *Acta Biomater*. 2015; 11:520. [PubMed: 25257316]
14. Alghamdi HS, Bosco R, Both SK, Lafisco M, Leeuwenburgh SC, Jansen JA, van den Beucken JJ. *Biomaterials*. 2014; 35:5482. [PubMed: 24731712]
15. Tan YF, Mundargi RC, Chen MHA, Lessig J, Neu B, Venkatraman SS, Wong TT. *Small*. 2014; 10:1790. [PubMed: 24510544]
16. Xiao W, Fu HL, Rahaman MN, Liu YX, Bal BS. *Acta Biomater*. 2013; 9:8374. [PubMed: 23747325]
17. Reardon PJT, Huang J, Tang JW. *Adv. Healthcare Mater*. 2013; 2:682.
18. Yang YH, Liu CH, Liang YH, Lin FH, Wu KCW. *J Mater. Chem. B*. 2013; 1:2447.
19. Ding XM, Zhu MF, Xu BS, Zhang JM, Zhao YH, Ji SL, Wang LN, Wang LY, Li XL, Kong DL, Ma XL, Yang Q. *ACS Appl. Mater. Inter*. 2014; 6:16696.
20. Tian Y, Jiang XJ, Chen X, Shao ZZ, Yang WL. *Adv. Mater*. 2014; 26:7393. [PubMed: 25238148]
21. Yucel T, Lovett ML, Giangregorio R, Coonahan E, Kaplan DL. *Biomaterials*. 2014; 35:8613. [PubMed: 25009069]
22. Kundu J, Chung Y, Kim YH, Tae G, Kundu SC. *Int. J. Pharm*. 2010; 388:242. [PubMed: 20060449]
23. Shi PJ, Abbah SA, Saran K, Zhang Y, Li J, Wong HK, Goh JCH. *Biomacromolecules*. 2013; 14:4465. [PubMed: 24224461]
24. Anumolu R, Gustafson JA, Magda JJ, Cappello J, Ghandehari H, Pease LF. *ACS Nano*. 2011; 5:5374. [PubMed: 21696150]
25. Shi PJ, Chen KL, Goh JCH. *Adv. Healthcare Mater*. 2013; 2:934.
26. He PF, Sahoo S, Ng KS, Chen KL, Toh SL, Goh JCH. *J Biomed. Mater. Res. Part A*. 2013; 101:555.
27. Huang XW, Liu X, Liu SS, Zhang AL, Lu Q, Kaplan DL, Zhu HS. *J Biomed. Mater. Res. Part B*. 2014; 102:1720.
28. Han FF, Liu SS, Pei YZ, Bai SM, Zhao HJ, Lu Q, Ma FG, Kaplan DL, Zhu HS. *Acta Biomater*. 2014; 10:921. [PubMed: 24090985]
29. Bai SM, Zhang WM, Lu Q, Ma QH, Kaplan DL, Zhu HS. *J Mater. Chem. B*. 2014; 2:6590.
30. Bai SM, Zhang XL, Lu Q, Sheng WQ, Liu LJ, Dong BJ, Kaplan DL, Zhu HS. *Biomacromolecules*. 2014; 15:3044. [PubMed: 25056606]
31. Yu SY, Yang WH, Chen S, Chen MJ, Liu YZ, Shao ZZ, Chen X. *RSC. Advances*. 2014; 4:18171.
32. Chen S, Shi XT, Osaka A, Gao H, Hanagata N. *Chem. Eng. J*. 2014; 246:1.
33. Zhang QC, Tan K, Zhang Y, Ye ZY, Tan WS, Lang MD. *Biomacromolecules*. 2014; 15:84. [PubMed: 24266740]
34. Bhakta G, Lim ZXH, Rai BN, Lin TX, Hui JH, Prestwich GD, van Wijnen AJ, Nurcombe V, Cool SM. *Acta Biomater*. 2013; 9:9098. [PubMed: 23871940]
35. Sailhan F, Gleyzolle B, Parot R, Guerini H, Viguier E. *Injury*. 2010; 41:680. [PubMed: 19880114]
36. Gloub EE, Boesze-Battaglia K. *Current Opinion in Orthopaedics*. 2007; 18:444.
37. Bhumiratana S, Grayson WL, Castaneda A, Rockwood DN, Gil ES, Kaplan DL, Vunjak-Novakovic G. *Biomaterials*. 2011; 32:2812. [PubMed: 21262535]

38. Lucero CMJ, Vega OA, Osorio MM, Tapia JC, Antonelli M, Stein GS, van Wijnen AJ, Galindo MA. *J Cell. Physiol.* 2013; 228:714. [PubMed: 22949168]
39. Gaharwar AK, Mihaila SM, Swami A, Patel A, Sant S, Reis RL, Marques AP, Gomes ME, Khademhosseini A. *Adv. Mater.* 2013; 25:3329. [PubMed: 23670944]
40. Park JS, Yang HN, Jeon SY, Woo DG, Na K, Park KH. *Biomaterials.* 2010; 31:6239. [PubMed: 20537381]
41. Li JJ, Gil ES, Hayden RS, Li CM, Roohani-Esfahani SI, Kaplan DL, Zreiqat H. *Biomacromolecules.* 2013; 14:2179. [PubMed: 23745709]

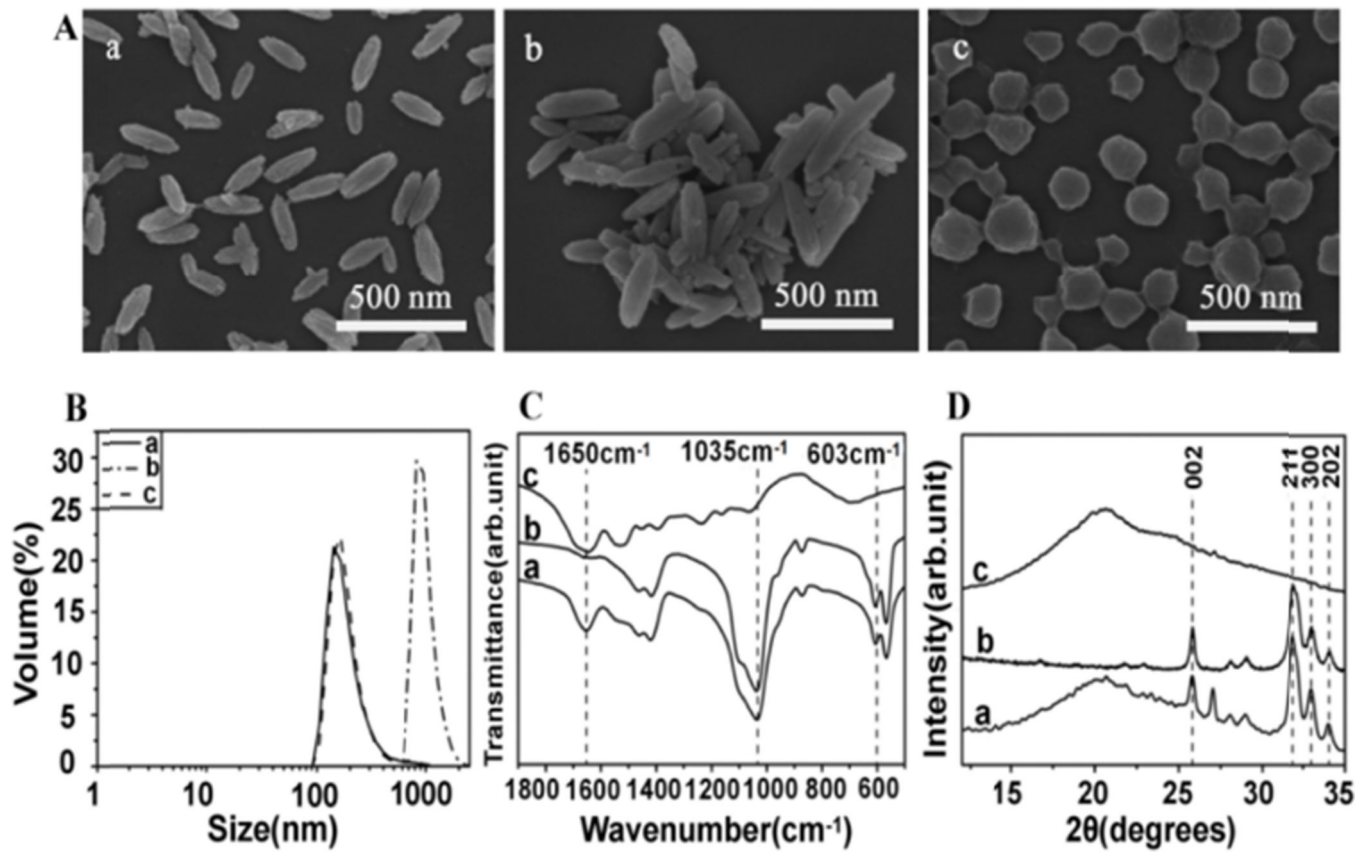


Figure 1. The characterization of different nanoparticles: (A) SEM morphology, (B) Size distribution, (C) FTIR spectra and (D) XRD patterns of silk-HA composite nanoparticles (a), HA nanoparticles (b) and silk nanoparticles (c).

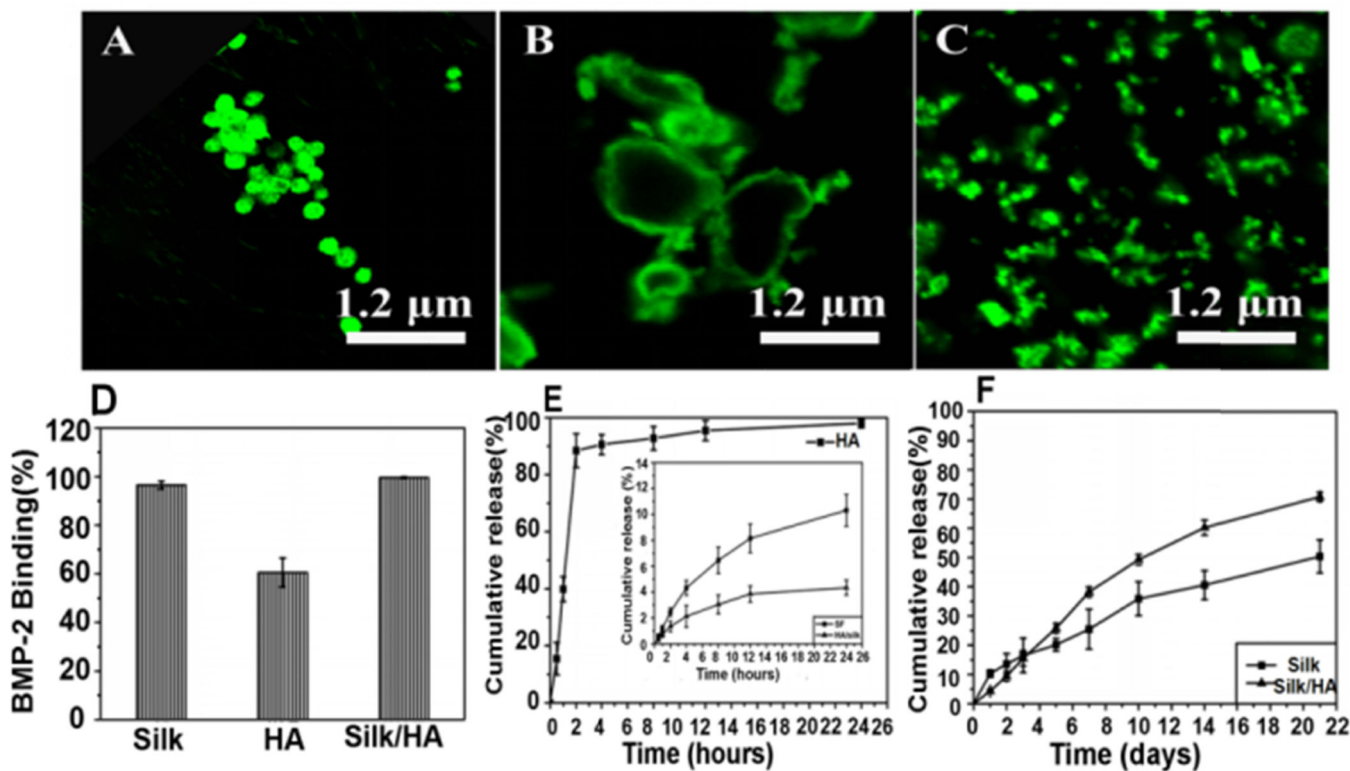


Figure 2.

BMP-2 loading and release from the different nanoparticles: (A) Fluorescent microscopy images for FITCBMP-2 (Green) loaded Silk nanoparticles, (B) Fluorescent microscopy images for FITCBMP-2 (Green) loaded HA nanoparticles, (C) Fluorescent microscopy images for FITCBMP-2 (Green) loaded Silk-HA composite nanoparticles, (D) Binding efficiency of BMP-2 on the different particles, and (E, F) BMP-2 release profiles from the different particles. Five replicate samples were used for each condition (n=5). The nanocarriers aggregated to some extent when loaded with B P-2, resulting in the increase of particle sizes.

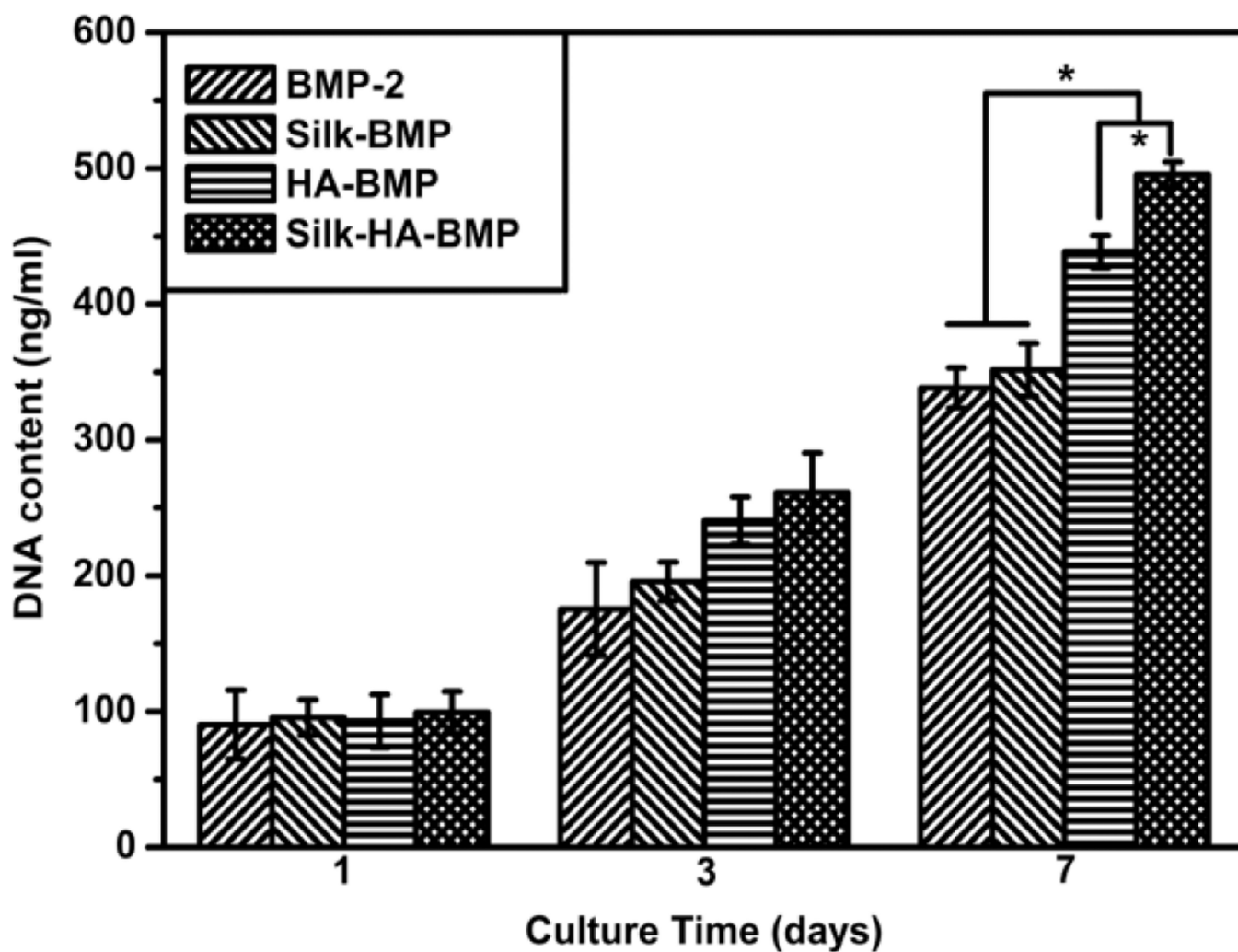


Figure 3. DNA assay of BMSCs cultured with different BMP-2 loaded nanoparticles. The samples were as follows: BMP-2, soluble BMP-2; Silk-BMP, BMP-2 loaded silk nanoparticles; HA-BMP, BMP-2 loaded HA nanoparticles; and Silk-HA-BMP, BMP-2 loaded silk-HA composite nanoparticles. Error bars represent mean \pm standard deviation with N=5 (*p < 0.05).

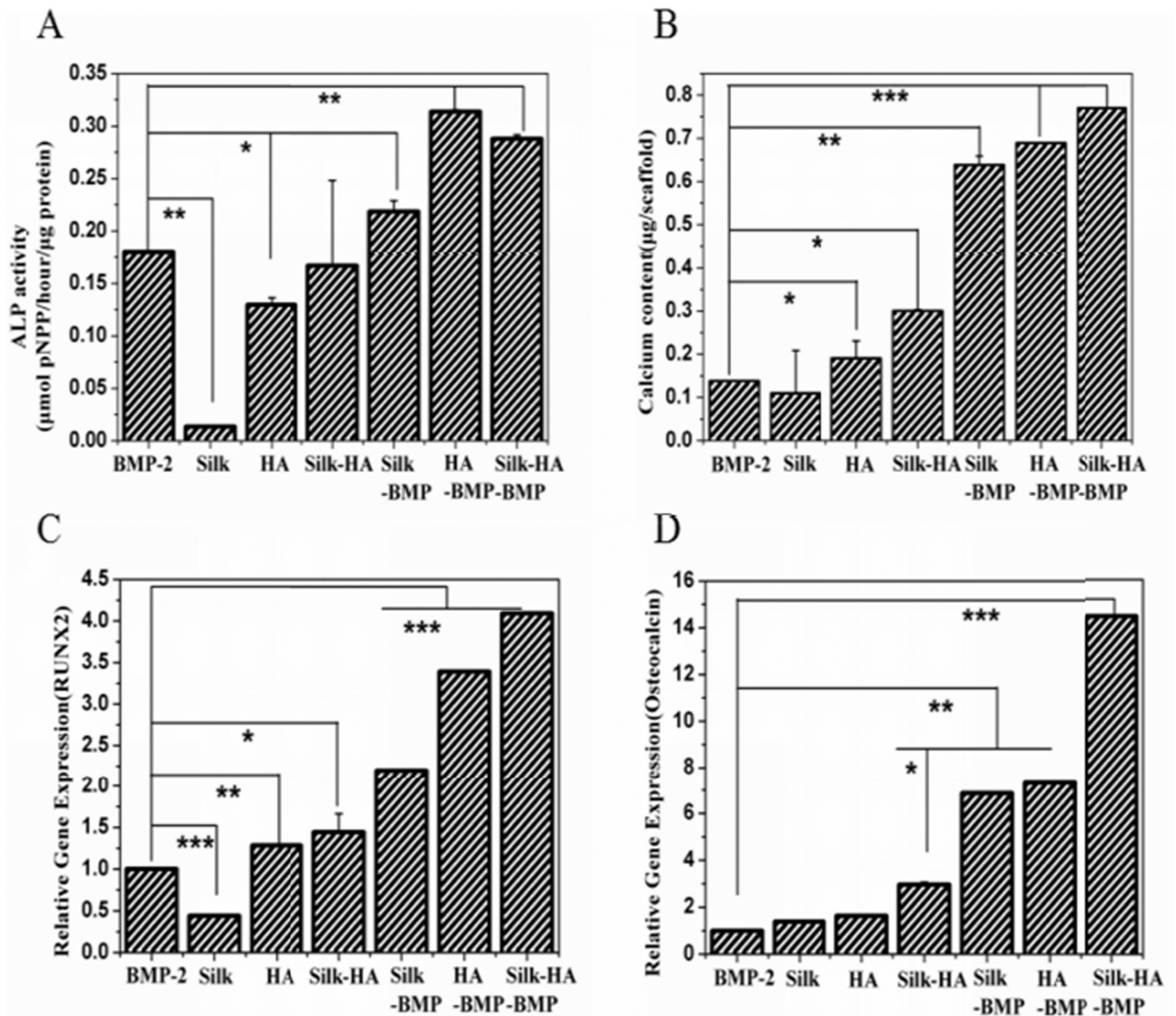


Figure 4.

Expression of osteogenic markers from BMSCs cultured with different nanoparticles for 1 week: (A) biochemical activity of alkaline phosphatase, (B) calcium content, (C) transcript expression of RUNX2 and (D) transcript expression of osteocalcin. The samples were as follows: BMP-2, soluble BMP-2; Silk, BMP-2 free silk nanoparticles; HA, BMP-2 free HA nanoparticles; Silk-HA, BMP-2 free silk-HA composite nanoparticles; HA-BMP, BMP-2 loaded HA nanoparticles; Silk-HA-BMP, BMP-2 loaded silk-HA composite nanoparticles and Silk-BMP, BMP-2 loaded silk nanoparticles (*p 0.05, and **P 0.01,***P 0.001).

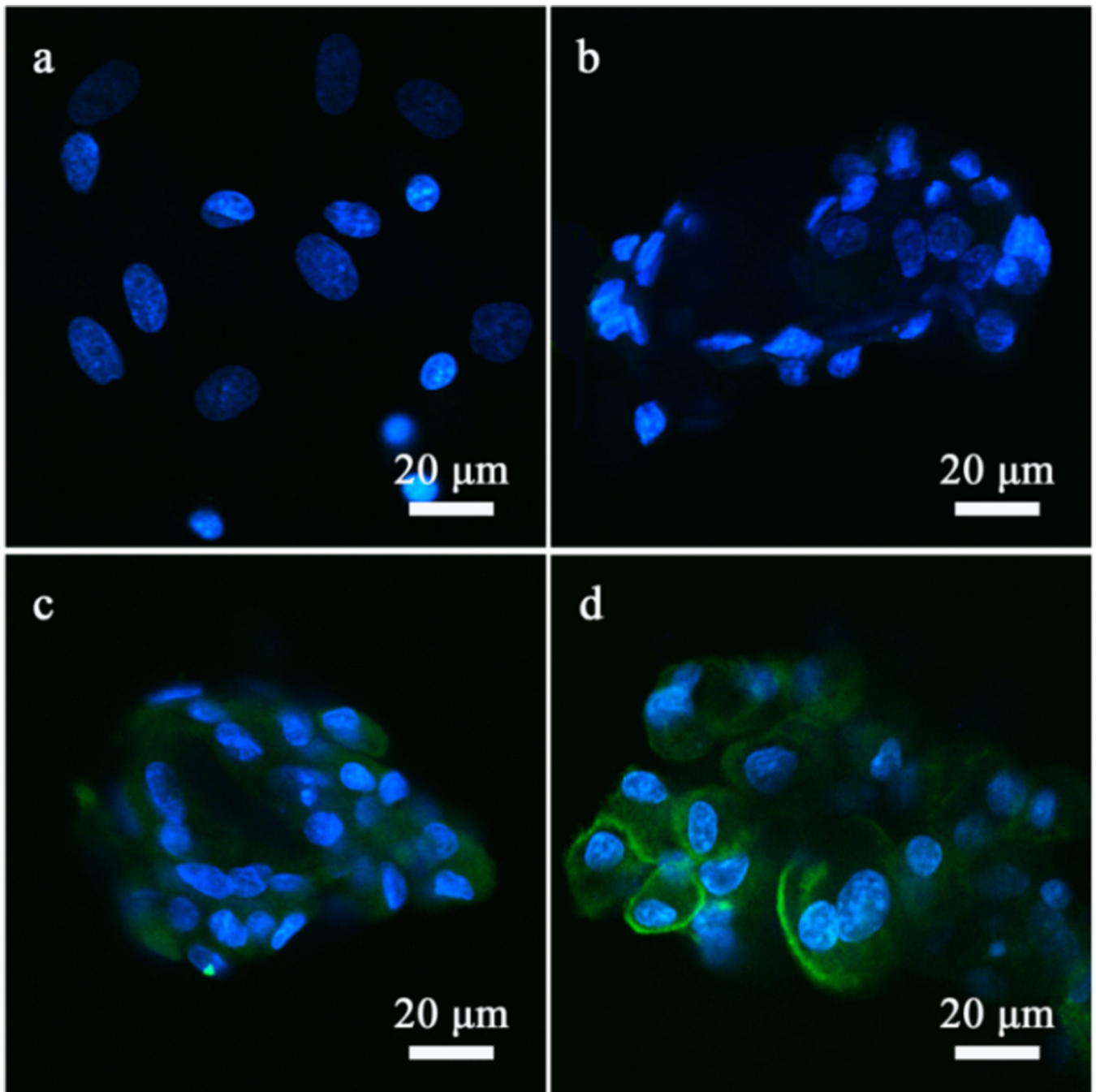


Figure 5. Immunofluorescence staining for collagen I of BMSCs cultured with soluble BMP-2 (a), BMP-2 loaded silk nanoparticles (b), BMP-2 loaded HA nanoparticles (c), and BMP-2 loaded silk-HA composite nanoparticles (d) for 1 week. The blue color (DAPI) represents cell nucleus, while the green color (FITC labeled phalloidin) represents the expression of specific marker protein collagen I.